

Improving Tissue Electrical Properties Reconstructions by Exploiting the Benefits of Combining Deep Learning-EPT and 3D Contrast Source Inversion-EPT

Reijer L. Leijsen¹, Cornelis A.T. van den Berg^{2,3}, Rob F. Remis⁴, Andrew G. Webb¹, and Stefano Mandija^{2,3}

¹Radiology, Leiden University Medical Center, Leiden, Netherlands, ²University Medical Center Utrecht, Utrecht, Netherlands, ³Utrecht University, Utrecht, Netherlands, ⁴Circuits and Systems Group, Delft University of Technology, Delft, Netherlands

Synopsis

We propose a two-step approach to EPT reconstruction where we use the results from a deep-learning approach as the initial estimate for a 3D contrast-source inversion algorithm. The combination of these two methods builds upon the strengths of each. Results using an anatomically accurate head model with and without an artificially inserted tumour show that CSI-EPT improves DL-EPT reconstructions in structures that are not present in the training set, while DL-EPT used as an initial guess for CSI-EPT leads to improved accuracy and convergence.

Introduction

Helmholtz-based EPT¹⁻³ (Helm-EPT) methods enable reconstructions of tissue electrical properties (EPs; conductivity σ and relative permittivity ϵ_r) from B_1^+ measurements. However, these reconstructions are severely affected by noise and tissue boundaries.

Recently, deep learning EPT⁴ (DL-EPT) has been shown to enable fast and noise-robust reconstructions with good correlation with tissue properties. However, DL-EPT reconstructions of tissue contrast/structures not present in the training set, e.g. pathological cases, still needs to be proven.

In parallel, it has been shown that a 3D implementation of contrast source inversion EPT^{5,6} (CSI-EPT) is able to accurately reconstruct tissue boundaries based on 3D B_1^+ fields. The performance of this method, however, depends highly on the initial estimate.

In this work, we propose a two-step approach where we use DL-EPT reconstructions as an initial estimate for CSI-EPT reconstructions. CSI-EPT is expected to improve DL-EPT reconstructions in structures not present in the training set, while DL-EPT used as an initial guess for CSI-EPT should improve the accuracy and convergence.

Methods

Helmholtz EPT¹⁻³ (Helm-EPT) was performed on noiseless, complex B_1^+ fields at 300 MHz simulated in Remcom⁷ using a birdcage coil and Duke head model (the Virtual Family⁸). Since Helm-EPT reconstructions are severely affected by the Laplacian operator, its resulting EP maps are constrained by minimum and maximum EP values and smoothed by a bilateral 5x5x5 exponential filter³ applied independently to each tissue type (white matter (WM), gray matter (GM) and cerebrospinal fluid (CSF)) to improve EPs reconstructions at tissue boundaries.

DL-EPT reconstructions were performed for the same head model (excluded from the training) using a conditional Generative Adversarial Network⁴ trained using complex B_1^+ fields simulated in Sim4Life⁹.

3-D CSI-EPT⁶ reconstruction was performed using as an initial guess (i) a homogeneous mask (hom-CSI, $\sigma = 0.6$, $\epsilon_r = 43$), (ii) Helm-EPT (Helm-CSI), or (iii) DL-EPT (DL-CSI). For each reconstruction, 10,000 iterations were performed, and a conjugate-gradient update approach for the contrast function was used to improve convergence.

The reconstruction accuracy is evaluated for each method in the WM, GM, and CSF.

Finally, to test robustness for independent data with pathology, we investigate the accuracy of these approaches in reconstructing the EPs of an artificially inserted tumour region in the Duke head model.

Results & Discussion

In Figures 1 and 2, EPs reconstructions and absolute error maps are shown for Helm-EPT, DL-EPT and CSI-EPT using the three different initializations. Mean absolute error values for WM, GM, and CSF are reported in Table 1.

Helm-EPT shows severe boundary errors. DL-EPT shows increased accuracy in the mean values, but errors are still present (e.g. boundary of the ventricles). Three-dimensional hom-CSI shows artefacts in homogeneous regions, for example WM. Helm-CSI shows better quality EPs maps, but the accuracy is severely affected by the intrinsic errors in Helm-EPT, especially at boundaries. The combination of DL and 3D CSI-EPT outperforms the other methods (globally the lowest mean absolute errors, see Table 1). The major error in the conductivity of the ventricles in DL-EPT and the error in the homogeneous region in hom-CSI are greatly reduced.

Figures 3 and 4 show EPs reconstructions and absolute error maps for the tumour model. Mean absolute errors for tumour EPs reconstructions are reported in Figure 4. Helm-EPT reconstructs the tumour, but the values are not accurate due to severe boundary errors. DL-EPT shows better accuracy, but the shape is not well reconstructed, likely because the network was not trained with tumour models. This highlights the need of an exhaustive training set for DL-EPT. Hom-CSI shows a better reconstruction of the tumour shape, but artificial bands occur in the tumour, corrupting the reconstruction. This improves for Helm-CSI, but the accuracy is poor, as previously observed. DL-CSI provides good quality and accurate EPs reconstruction of the tumour (relative error percentage of both EPs approximately 10%).

Conclusion

By taking a DL-EPT reconstruction as an initial guess for CSI-EPT, improved tissue reconstructions are obtained. On one hand, CSI-EPT improves DL-EPT reconstructions since it explicitly takes Maxwell's equations, governing the electromagnetic field behaviour, into account. On the other hand, CSI-EPT reconstructions are improved, since an initial guess based on DL-EPT leads to reconstructions with higher accuracy and improved convergence rate compared to CSI-EPT reconstructions obtained using as initial guess a homogeneous EPs model or Helm-EPT reconstructions.

Acknowledgements

The research of R.L. Leijsen was funded by European Research Council Advanced NOMA MRI under grant number 670629.

References

- ¹Haacke EM, Petropoulos LS, Nilges EW, Wu DH. Extraction of conductivity and permittivity using magnetic resonance imaging. *Phys Med Biol.* 1991;36(6):723-734.
- ²Katscher U, Voigt T, Findekklee C, et al. Determination of Electric Conductivity and Local SAR Via B1 Mapping, *IEEE Tran Med Im.* 2009;28(9):1365-1374.
- ³Katscher U, van den Berg CAT. Electric properties tomography: Biochemical, physical and technical background, evaluation and clinical applications. *NMR Biomed.* 2017;30(8):e3729.
- ⁴Mandija S, Meliador EF, Huttinga NRF, et al. Opening a new window on MR-based Electrical Properties Tomography with deep learning. *arXiv:1804.00016*, 2018;
- ⁵van den Berg PM, Abubakar A. Contrast source inversion method: State of art. *Prog Electromagn Res.* 2001;34(11):189-218.
- ⁶Leijsen RL, Brink WM, van den Berg CAT, et al. 3-D Contrast Source Inversion-Electrical Properties Tomography. *IEEE Tran Med Im.* 2018;37(9):2080-2089.
- ⁷XFdtd, Remcom State College, PA, USA.
- ⁸Christ A, Kainz W, Hahn EG, et al. The virtual family development of surface-based anatomical models of two adults and two children for dosimetric simulations. *Phys Med Biol.* 2010;55(2):23-38.
- ⁹Sim4Life, ZMT AG, Zurich, CH.

Figures

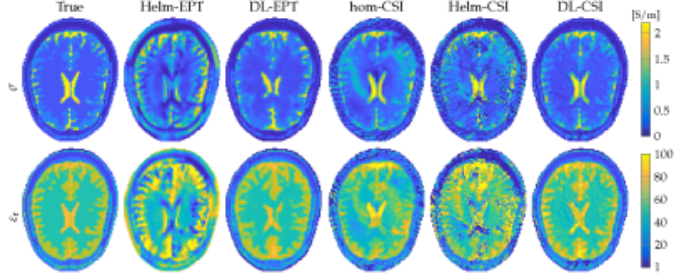


Figure 1: Results from different EPT reconstruction methods. From left to right: True model, Helmholtz EPT (Helm-EPT), deep learning EPT (DL-EPT), and 3D CSI-EPT with homogeneous initialization (hom-CSI), with Helmholtz-EPT initialization (Helm-CSI) and deep learning initialization (DL-CSI).

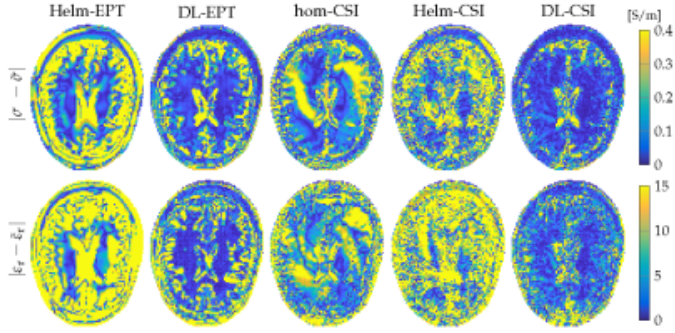


Figure 2: Absolute error maps of the reconstructions from the different EPT approaches shown in Figure 1.

Conductivity					
	Helm-EPT	DL-EPT	hom-CSI	Helm-CSI	DL-CSI
WM	0.2162	0.1332	0.2278	0.8921	0.0645
GM	0.3577	0.2640	0.4212	0.8088	0.1385
CSF	0.8893	0.6145	1.2215	0.5206	0.3494
Permittivity					
	Helm-EPT	DL-EPT	hom-CSI	Helm-CSI	DL-CSI
WM	13.6966	6.8144	9.2524	14.7035	3.8877
GM	23.8229	6.6067	15.9921	21.5699	5.7839
CSF	22.7999	4.7418	21.4785	41.7797	8.1046

Table 1: Mean absolute errors over the 3D segmented regions: WM, GM and CSF.

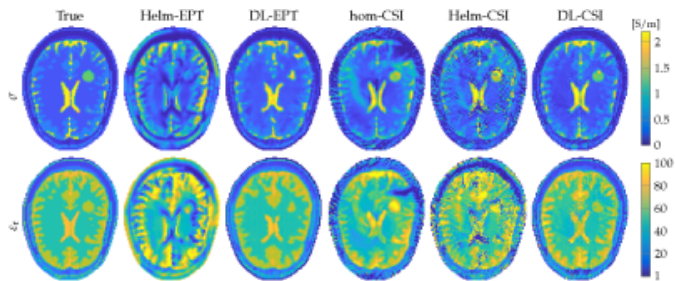


Figure 3: Results from different EPT reconstruction methods, for the Duke model containing an artificial tumour.

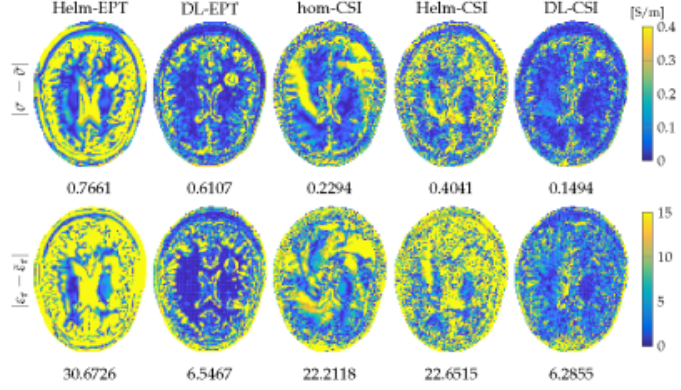


Figure 4: Absolute error maps of the reconstructions from different EPT approaches, for the Duke model containing an artificial tumour. The numbers denote the absolute error of the tumour only.